nature cell biology

Genome-wide RNAi screening identifies human proteins with a regulatory function in the early secretory pathway

Jeremy C. Simpson[1,7], Brigitte Joggerst[2], Vibor Laketa[2], Fatima Verissimo[2], Cihan Cetin[2], Holger Erfle[2,6], Mariana G. Bexiga[1], Vasanth R. Singan[1], Jean-Karim Hériché[3], Beate Neumann[3], Alvaro Mateos[2], Jonathon Blake[4], Stephanie Bechtel[5], Vladimir Benes[4], Stefan Wiemann[5], Jan Ellenberg[2,3] and Rainer Pepperkok[2,7]

The secretory pathway in mammalian cells has evolved to facilitate the transfer of cargo molecules to internal and cell surface membranes. Use of automated microscopy-based genome-wide RNA interference screens in cultured human cells allowed us to identify 554 proteins influencing secretion. Cloning, fluorescent-tagging and subcellular localization analysis of 179 of these proteins revealed that more than two-thirds localize to either the cytoplasm or membranes of the secretory and endocytic pathways. The depletion of 143 of them resulted in perturbations in the organization of the COPII and/or COPI vesicular coat complexes of the early secretory pathway, or the morphology of the Golgi complex. Network analyses revealed a so far unappreciated link between early secretory pathway function, small GTP-binding protein regulation, actin cytoskeleton organization and EGF-receptor-mediated signalling. This work provides an important resource for an integrative understanding of global cellular organization and regulation of the secretory pathway in mammalian cells.

Within higher eukaryotic cells membrane traffic pathways connect the various membrane-bounded organelles, thereby ensuring that they retain the correct complement of proteins and lipids to maintain cellular homeostasis. Typically, membrane traffic steps do not work in isolation, but rather are linked together in a carefully ordered sequence of events. The paradigm of this is the constitutive secretory pathway, which ensures that newly synthesized material originating at the endoplasmic reticulum (ER) is correctly modified as it passes through the Golgi complex and ultimately out to the cell surface. This pathway has the capacity to cope with a variety of cargo molecules, and as such utilizes an extensive array of regulatory machinery[1,2]. At the heart of this machinery are cytoplasmic coat protein complexes that identify cargo, reshape membranes into transport carriers and provide links to other accessory proteins. In the early secretory pathway it is the COPII and COPI coat complexes that perform these roles[3,4], and therefore a greater understanding of their functional networks is a vital step towards understanding the regulation of the entire secretion process.

Extensive efforts over many years have revealed a significant number of regulators associated with the secretory pathway. Early biochemical approaches to identify individual machinery components have started to make way for more systematic strategies, including organellar proteomics and high-throughput imaging-based methods, in an effort to complete the cataloguing process[5,6]. More recently, RNA interference (RNAi)-mediated gene knockdown has been the method of choice, including two genome-wide secretion screens, in *Drosophila* cells[7,8]. Although these screens revealed several regulatory candidates, a significant fraction (approximately 40%) do not seem to have a human orthologue. Therefore, to discover how the secretion process is finely tuned in human cells, we ideally require use of a human cell system. Largely as a result of the complex genetic architecture of mammalian systems, genome-wide RNAi screens in human cells are still relatively few in number. Indeed with regard to membrane traffic, the screens reported so far have targeted specific gene families[9,10]. We have previously described a fully automated high content screening RNAi-based approach to quantitatively monitor membrane transport in cultured

[1]School of Biology and Environmental Science & Conway Institute of Biomolecular and Biomedical Research, University College Dublin (UCD), Dublin 4, Ireland. [2]Cell Biology and Biophysics Unit, European Molecular Biology Laboratory (EMBL), Meyerhofstrasse 1, 69117 Heidelberg, Germany. [3]MitoCheck Project Group, EMBL, Meyerhofstrasse 1, 69117 Heidelberg, Germany. [4]Gene Core, EMBL, Meyerhofstrasse 1, 69117 Heidelberg, Germany. [5]Division of Molecular Genome Analysis, German Cancer Research Centre (DKFZ), Im Neuenheimer Feld 580, 69120 Heidelberg, Germany. [6]Present address: BioQuant Centre, University of Heidelberg, Im Neuenheimer Feld, 69120 Heidelberg, Germany.
[7]Correspondence should be addressed to J.C.S. or R.P. (e-mail: jeremy.simpson@ucd.ie or pepperko@embl.de)

Received 13 January 2012; accepted 26 April 2012; published online 3 June 2012; DOI: 10.1038/ncb2510

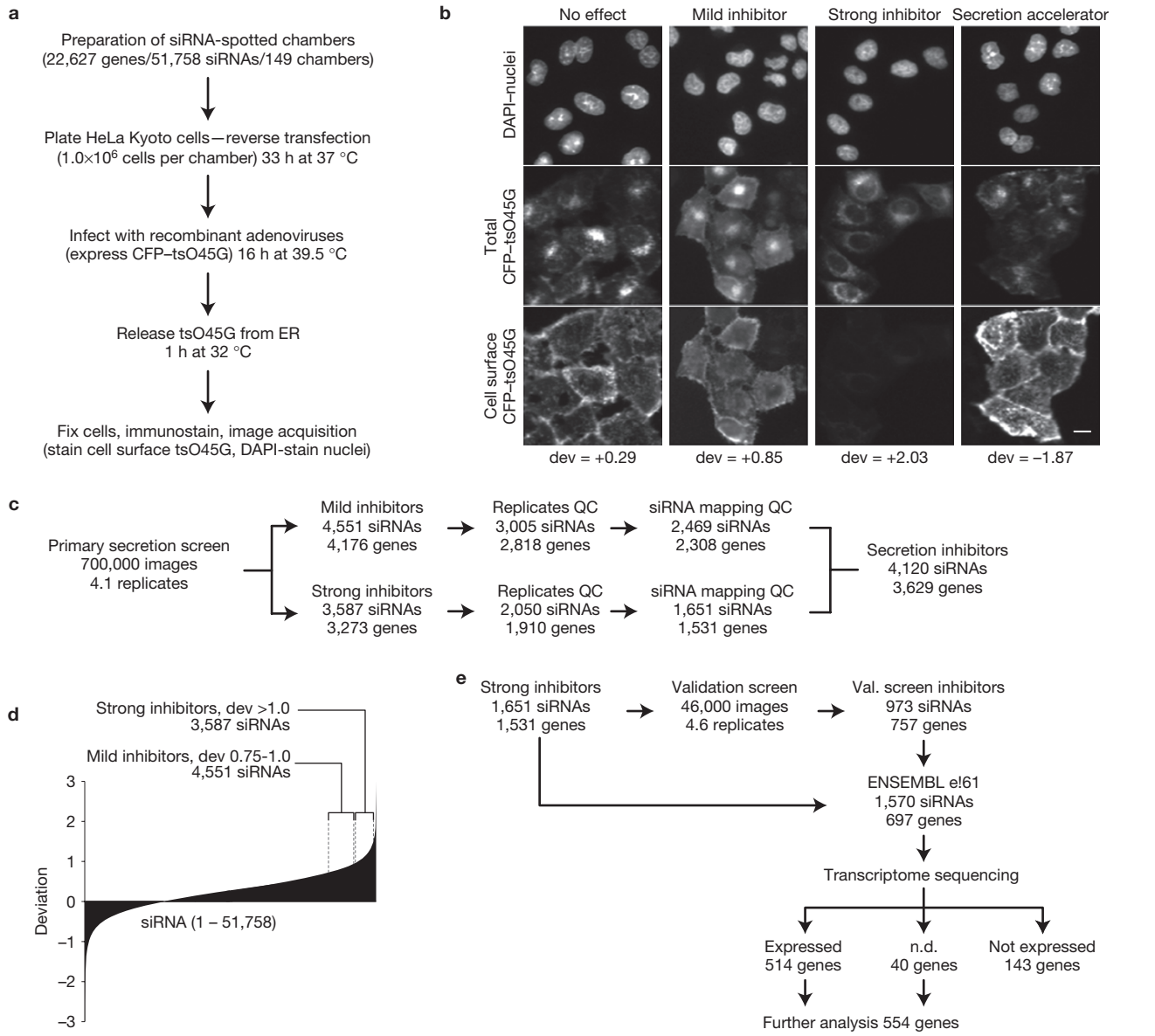

Figure 1 Primary and validation secretion screens in HeLa cells. (**a**) Overview of experimental approach to monitor cell surface arrival of tsO45G in downregulated cells. (**b**) Example images of cells showing either no effect, mild inhibition, strong inhibition or acceleration of secretion. Scale bar, 10 μm. (**c**) Results pipeline from primary secretion screens indicating quality control (QC) steps employed. From 22,627 genes, a total of 3,629 genes were found to inhibit secretion on knockdown. See also Supplementary Table S1. (**d**) Graphical overview of effect on secretion of genome-wide siRNA set used in this study (primary screen). Deviation values of 0.75–1.0 were considered mild inhibitors; deviations >1.0 were considered strong inhibitors. (**e**) Results pipeline from validation secretion screens employing further siRNA sequences against each target gene identified in the primary screen. Genes were considered as validated hits (697 genes) when secretion could be inhibited by deviation values >1.0 with two or more independent siRNAs. Whole transcriptome sequencing established that 143 of these were not expressed at detectable levels within the cells, and these candidates were not included in further analyses. The remaining expressed genes (514) and those that were not analysed in the transcriptome sequencing (40) were taken into secondary screens for further analysis. See also Supplementary Tables S4 and S5.

human cells[11], specifically assessing the arrival of a fluorescently labelled transmembrane cargo protein at the cell surface. Here we apply and extend this approach, providing the first systematic survey of the human genome with respect to the constitutive secretion process.

RESULTS

Genome-wide cell-based secretion screening

We used our previously described RNAi-based high content screening microscopy platform[11] to screen a genome-wide library of over 51,000 small interfering RNAs (siRNAs) targeting approximately 22,000 human genes[12] for interference with ER-to-plasma membrane transport of the well-characterized secretory cargo membrane protein tsO45G (ref. 13). This approach allows single-cell quantification of the relative levels of fluorescently labelled tsO45G both inside the cell and at the plasma membrane (Fig. 1a,b). In total 700,000 images (representing on average 4.1 replicates per siRNA) containing in total 8.3 million cells were automatically acquired and transport of tsO45G to the plasma membrane was quantified[11]. We classified the secretion inhibitors as either mild (deviation 0.75–1.0) or strong (deviation >1.0) inhibitors (Fig. 1c,d). After taking account of replicate reproducibility

and siRNA mapping (to ENSEMBL 61), the number of mild inhibitory siRNAs was determined to be 2,469 siRNAs targeting 2,308 genes, and the number of strong inhibitory siRNAs was 1,651 siRNAs targeting 1,531 genes. Compiling these data together revealed a final list of 3,629 genes, which on downregulation resulted in a marked inhibition of transfer of tsO45G to the cell surface (Supplementary Table S1 and www.mitocheck.org). A further 230 siRNAs accelerated tsO45G transport, but were not studied further (Supplementary Table S2); and 384 siRNAs consistently resulted in too few cells remaining at the end of the experiment for reliable quantification, and could not be assessed (Supplementary Table S3).

Following the primary screen, we initially focused on those 1,531 genes that caused the most significant inhibition of secretion on knockdown. Using independent siRNA sequences targeting these genes, we tested for their interference with tsO45G transport, in so-called validation screens. In total, we identified 697 genes for which a minimum of two independent siRNAs from the primary and validation screens, but in some cases three or even four independent siRNAs, caused transport inhibition. Whole genome transcriptome sequencing revealed 514 from the 697 candidate genes as being clearly expressed in the HeLa cells used in our screens. For a further 40 genes we were unable to generate any definitive transcriptome data. The genes from both of these groups are hereafter referred to as hit genes (Fig. 1e and Supplementary Table S4). For 143 of our candidate genes we consistently obtained expression levels below our detection threshold (Supplementary Table S5), indicating that they were either absent from our cells or present in too low abundance to be detected. Although we consider the latter possibility more likely, as for all of them secretion inhibition with two or more independent siRNAs was obtained in our screens, the secretion phenotypes recorded for these genes may have occurred as a result of off-target effects of these siRNAs. Therefore, to provide the maximum confidence in the gene lists used for subsequent experiments, these candidates were not further studied.

Identification of known membrane traffic machinery

Following folding in the ER, secretory cargo is concentrated at ER exit sites. This process is largely driven through the multi-subunit cytoplasmic coat complex COPII (ref. 14), and a number of associated regulators (Supplementary Table S6). We therefore examined our primary secretion screen data for the effect of depletion of COPII subunits on tsO45G secretion. Consistent with a previous report demonstrating that double knockdowns of the SEC24 COPII subunit isoforms were necessary to impair ER–Golgi trafficking in HeLa cells[15], we also did not detect significant secretion inhibition on knockdown of individual COPII subunits despite most of these siRNAs reducing target messenger RNA levels to below 20% of those measured in control cells (Fig. 2a and Supplementary Table S6). Combined knockdown of multiple COPII subunits did however result in strong transport inhibition (Fig. 2c), highlighting the need for greater understanding of the relative roles that different isoforms can play in multi-subunit complexes.

Secretory transport carriers en route to the Golgi rapidly shed their COPII coat and in turn become coated with the COPI coat[16,17]. Our primary secretion screen revealed that siRNAs targeting five of the seven COPI vesicular coat subunits (COPA, COPB2, COPD/ARCN1, COPG and the COPB used as a positive control) resulted in a marked inhibition of tsO45G transport (Fig. 2b and Supplementary Table S6). This increased detection of COPI subunits, compared with COPII subunits, most likely reflects that isoforms exist for only two of the COPI subunits, and that all conventional secretory cargo must pass through the Golgi complex, which itself is coated with COPI.

Individual cellular trafficking steps are also regulated through small GTPases of the ARF and Rab families, in addition to the SNARE fusion proteins, together termed the membrome[18]. Downregulation of the ARF family of GTPases showed four members as mild transport inhibitors, and only one member (ARF3) as a strong inhibitor. Of the 58 Rab GTPases assessed, 23 were inhibitors, including Rabs known to be associated with the secretory process; for example, RAB18 (ref. 19) and RAB1A (ref. 20). From the 35 SNAREs tested in our screen, 11 were found to inhibit secretion on knockdown, with six of these genes also reported in a previous screen as being important for secretion[10] (Supplementary Fig. S1 and Table S6).

Next, we looked at the importance of a key Rab regulator, the Rab GDP-dissociation inhibitor protein (GDI), to the secretory transport process. This protein is believed to play a key role in ensuring that Rabs are delivered to membranes in a timely fashion[21]. Our screen revealed that depletion of GDI1 generally resulted in a stronger secretion inhibition than depletion of GDI2. Consistent with the studies on COPII subunits, when we used siRNAs to simultaneously target pairs of genes (encoding GDI1 and GDI2), we observed a strong inhibition with all combinations of oligonucleotides tested (Fig. 2d).

Overall, when examining our results in the context of 171 well-established core membrane traffic machinery molecules, we were able to confirm the contribution of 59 molecules (35%) to secretion (Supplementary Table S6). The observation that we did not find a number of core machinery molecules (for example, COPII subunits) suggests that in mammalian systems the high degree of redundancy ensures the robustness of secretory function.

Role of secretion regulators in other cellular processes

We next analysed our data in the context of the two reported genome-wide loss-of-function screens for secretory transport performed in *Drosophila* S2 cells[7,8]. In the first study[7], of the 130 genes identified we were able to identify 80 with likely human orthologues for which we had RNAi data. Comparison with these data revealed an overlap of 15 genes that caused transport inhibition in both screens (Fig. 3a and Supplementary Table S7). A more recent study reported a total of 306 hit genes associated with secretion[8], from which we could identify 185 with human orthologues, and an overlap of 33 from our screen (Fig. 3a and Supplementary Table S7). Considering all three secretion screens together, only three genes were common to all (those encoding RAB1B; ref. 22; STX18; ref. 23; and USE1; ref. 24). Interestingly, USE1 has recently been reported to be essential for the maintenance of ER morphology[25], probably through interactions with its cognate partners, in particular STX18.

Although the overlap between the screens seems to be low, the studies in fly cells used soluble cargoes compared with the transmembrane cargo used in our work. A further explanation may be that the fly-cell studies used a five-day siRNA-mediated gene knockdown, compared with the two days in this study, resulting in distinct efficiencies in gene knockdowns between the screens, and also in different degrees of cell death induced by prolonged knockdown of essential genes. Also, despite

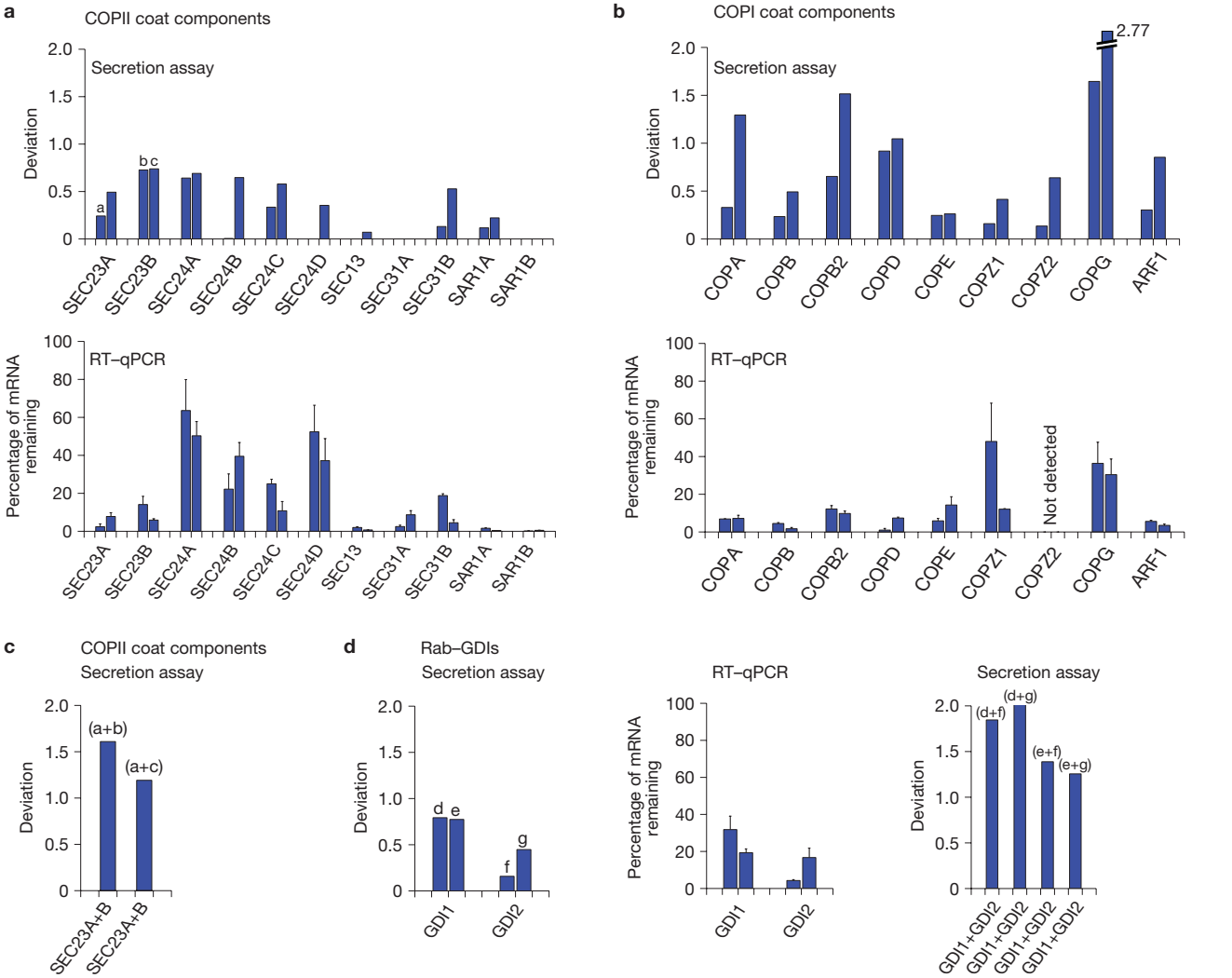

Figure 2 Analysis of well-known membrane traffic regulators in the secretion screens. (**a**) Secretion screen results for components of the COPII vesicular coat complex (top) and the effectiveness of their downregulation as judged by RT–qPCR (bottom). Letters a–c indicate the specific siRNAs used in the experiments shown in **c**. (**b**) Secretion screen results for components of the COPI vesicular coat complex (top) and the effectiveness of their downregulation as judged by RT–qPCR (bottom). (**c**) Analysis of the effect of combining siRNAs targeting two components of the COPII vesicular coat complex on secretion. (**d**) Secretion screen results for the two human Rab–GDI molecules associated with Rab GTPase function (left) and the effectiveness of their downregulation as judged by RT–qPCR (middle). Right, analysis of the effect on secretion of combining siRNAs targeting both Rab–GDI molecules simultaneously. Letters d–g indicate the specific siRNAs used. In all panels the individual bars represent data from individual siRNAs unless otherwise denoted. For RT–qPCR experiments the bars indicate mean and standard deviations between replicate experiments ($n = 3$). See also Supplementary Fig. S1 and Table S6.

only 45 of the genes we identified appearing in the candidate gene lists from fly cells, in fact the overlap between the two fly screens themselves was only 19 genes. Taken together, this highlights the fact that even modest differences in screening approach can result in the identification of distinct sets of candidate genes. In addition, the quality control and filtering steps used at various stages of an RNAi screen also differ significantly between screens, resulting in diverse hit lists. On this point, the design of appropriate and targeted secondary screens is essential.

We next examined the potential role of the genes we had identified in the context of other reported RNAi screens. Comparing our data with a live-cell screen for human genes involved in cell death, cell division and motility[12] revealed that 655 (18%) of our primary secretion screen inhibitors caused either cell death, mitotic defects or motility defects (Fig. 3b and Supplementary Table S8). Bioinformatic assessment of these genes showed that many of them participate in fundamental cellular processes such as transcription, providing an explanation why the knockdown of these genes caused cell death and most likely transport inhibition as a consequence. Depletion of numerous well-established membrane traffic regulators, such as the COPI subunits COPB2 and COPD/ARCN1, caused cell death, thus underlining the importance of the secretory pathway for general cell health.

Membrane traffic pathways are also regulated through the activities of kinases and phosphatases, with one recent study identifying 122 such genes being involved in ER–Golgi recycling[9]. We found that 39% (48 genes) of these genes also scored as secretion inhibitors in our study (Fig. 3c and Supplementary Table S9). We would not have expected a greater overlap between the screens, as our approach specifically assessed anterograde activity, whereas the kinase/phosphatase screen measured bi-directional transport between these organelles.

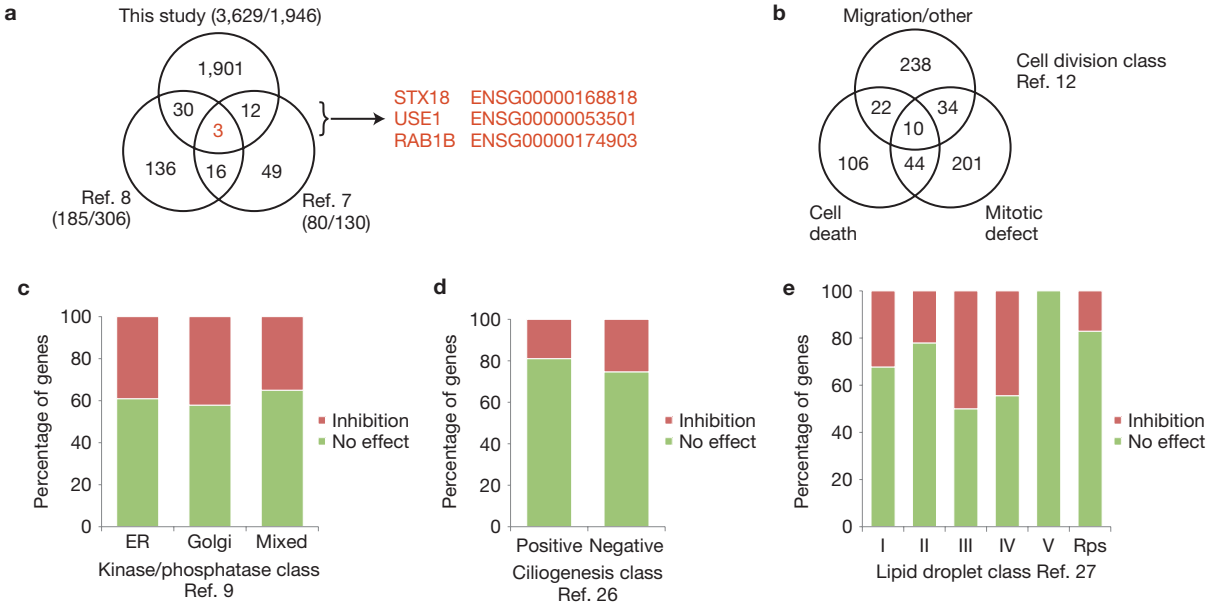

Figure 3 Comparison with data from other large-scale phenotypic screens. (**a**) Secretion screen results from mammalian cells compared with results obtained from similar secretion screens in *Drosophila* cells. The Venn diagram indicates the overlap of inhibitors between this screen in which 3,629 genes were initially detected and for which 1,946 *Drosophila* orthologues could be identified with secretion screens reported in fly cells[7,8]. In the cases of the screens in fly cells the values indicate the number of human orthologues as a proportion of the total number of secretion inhibitors reported in these screens. Only three genes were found to be common to the inhibitor lists across all three screens. See also Supplementary Table S7. (**b**) Further phenotypic effects recorded for the 3,629 genes identified in this screen as observed in the cell division screens[12]. See also Supplementary Table S8. (**c**) Comparison with the 122 kinase/phosphatase genes identified as being important for trafficking and organelle morphology in the early secretory pathway[9]. The classes ER/Golgi/Mixed are described elsewhere[9]. See also Supplementary Table S9. (**d**) Comparison with the 153 positive regulators and 79 negative regulators of ciliogenesis[26]. See also Supplementary Table S10. (**e**) Comparison to the genes found to affect lipid droplet morphology[27]. The phenotypic classes are described in that work. See also Supplementary Table S11.

We next compared our results with those obtained in a recent study examining genes involved in biogenesis of primary cilia[26], a process also dependent on membrane traffic activity. In this work, hits were classified as either positive (153 genes) or negative (79 genes) regulators. We detected only a relatively modest overlap of candidate genes between the screens (29 and 20 genes for each class respectively, representing 21% overlap overall; Fig. 3d and Supplementary Table S10). A number of these gene products are associated with membrane traffic, for example ARF4, RAB11B and RAB13, and probably act both as regulators of general constitutive secretion and in the transport of specialized ciliary components.

Finally we compared our results with those of a screen for lipid-droplet formation in *Drosophila* S2 cells[27]. Lipid droplets, at least in yeast, are functionally linked with the ER (ref. 28), and so there could be an overlap between genes involved in their formation and early secretory pathway function. From the 180 genes manually recorded as producing phenotypic effects on lipid-droplet morphology[27], 40 (22%) were recorded as inhibiting secretion (Fig. 3e and Supplementary Table S11). The degree of overlap we observed was highly dependent on the particular phenotype class recorded in the lipid-droplet screen, with the greatest overlap (4/8 genes, 50%) representing genes causing more dispersed lipid droplets of slightly larger size. This class was found to contain components of the COPI coat complex.

Subcellular localizations of secretion regulators

We next decided to gather more experimental data on the function of our candidate genes, focusing our efforts on those 1,531 genes that on knockdown resulted in the strongest secretion inhibition (Fig. 1c). Subcellular localization is an important determinant towards ascertaining function[29], and various methods exist to generate such information. One option is the use of antibodies and immunofluorescence analysis; however, extreme care must be taken when analysing subcellular patterns from fixed cells owing to the potential introduction of artefacts from the fixation and permeabilization processes[30]. An alternative method is the use of GFP-tagging of the respective open reading frames (ORFs), followed by their expression and observation in living cells[30,31]. In total we tagged 179 ORFs both at the amino and carboxy termini with GFP variants[31], transfected them into HeLa cells and observed the localizations of the fusion proteins in live cells. Of the 179 ORFs (prioritized by novelty with respect to secretion and availability of complementary DNAs) analysed in this way, 148 (83%) were also recorded as hit genes in our validation screen and transcriptome sequencing experiments. Creating both N- and C-terminal fusions was important, as 36 (20%) of the localizations observed were inconsistent between the two fusion orientations, and therefore having experimental data from both constructs was useful in guiding our final localization annotations (Fig. 4 and Supplementary Table S12). These experiments revealed a variety of localization patterns including soluble/cytoplasmic distributions, organelles of the endomembrane system and cytoskeleton-like elements (Fig. 4a,b). One protein (CLIC2) was present on short filaments distributed throughout the cytoplasm in living cells (Fig. 4b); however, on fixation most of these structures were lost, and co-stainings revealed only minor co-localization with the actin cytoskeleton (not shown). CLIC2 is a

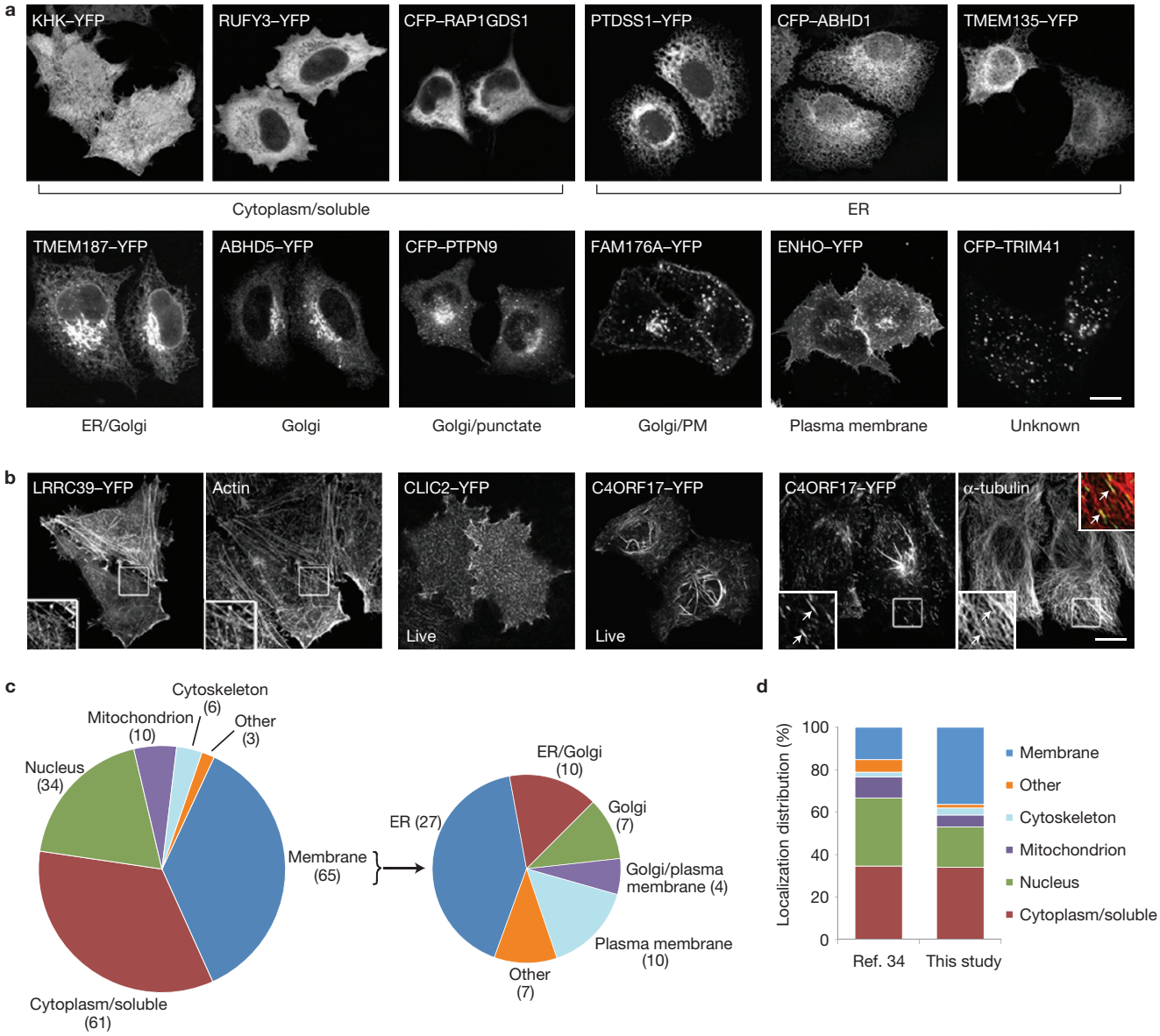

Figure 4 Analysis of the subcellular localization of candidates identified in the secretion screens. (**a**) Example confocal microscopy images of HeLa cells expressing a number of the fluorescently tagged proteins corresponding to the genes identified in the secretion screens. (**b**) Example images of cells showing proteins associated with cytoskeletal elements. Co-stainings with phalloidin (marking the actin cytoskeleton) or α-tubulin (marking the microtubule cytoskeleton) are also shown. Scale bars, 10 μm. (**c**) Overview of recorded subcellular localizations as determined by GFP-tagging of 179 proteins identified in the secretion screens. See also Supplementary Table S12. (**d**) Relative distribution of the localizations of the 179 genes inhibiting secretion and GFP-tagged in this study, compared with the genome-wide analysis of protein localization recorded in budding yeast[34].

member of a family of intracellular chloride channels, and has recently been reported to interact with ryanodine receptors[32], implying a role in calcium signalling. The subcellular localization of fluorescently tagged CLIC2 has not been reported, although other CLIC family members are associated with the actin cytoskeleton[33]. Three proteins seemed to be microtubule-associated, but of these only KIF2C and MARK2 showed clear co-localization with microtubule markers (not shown). C4ORF17 exhibited a complex pattern, being present on short filaments and intense filamentous bundles in both live and fixed cells, but the co-localization with microtubule markers was only partial (Fig. 4b).

Strikingly, the most represented class of localization observed was that of endomembrane organelles (denoted membrane; 65 proteins, 36%; Fig. 4c). The endomembrane proteins were further subdivided into classes associated with the various organelles of the secretory pathway, revealing that proteins associated with the ER and Golgi complex were the most abundant. Although there is still no experimental data with respect to subcellular localization of the entire human proteome, ORF–GFP localization data are available for more simple eukaryotes, namely budding yeast[34] and fission yeast[35]. We therefore compared our localization distribution with that of the proteins found in *Saccharomyces cerevisiae*, as determined by ORF GFP-tagging[34]. Although the proportion of proteins showing a soluble/cytoplasmic localization was similar between the two studies (34% and 35% respectively), it was striking that we observed a 2.4-fold higher fraction (36% versus 15%) of proteins localizing to the endomembrane system in our data set, compared with that

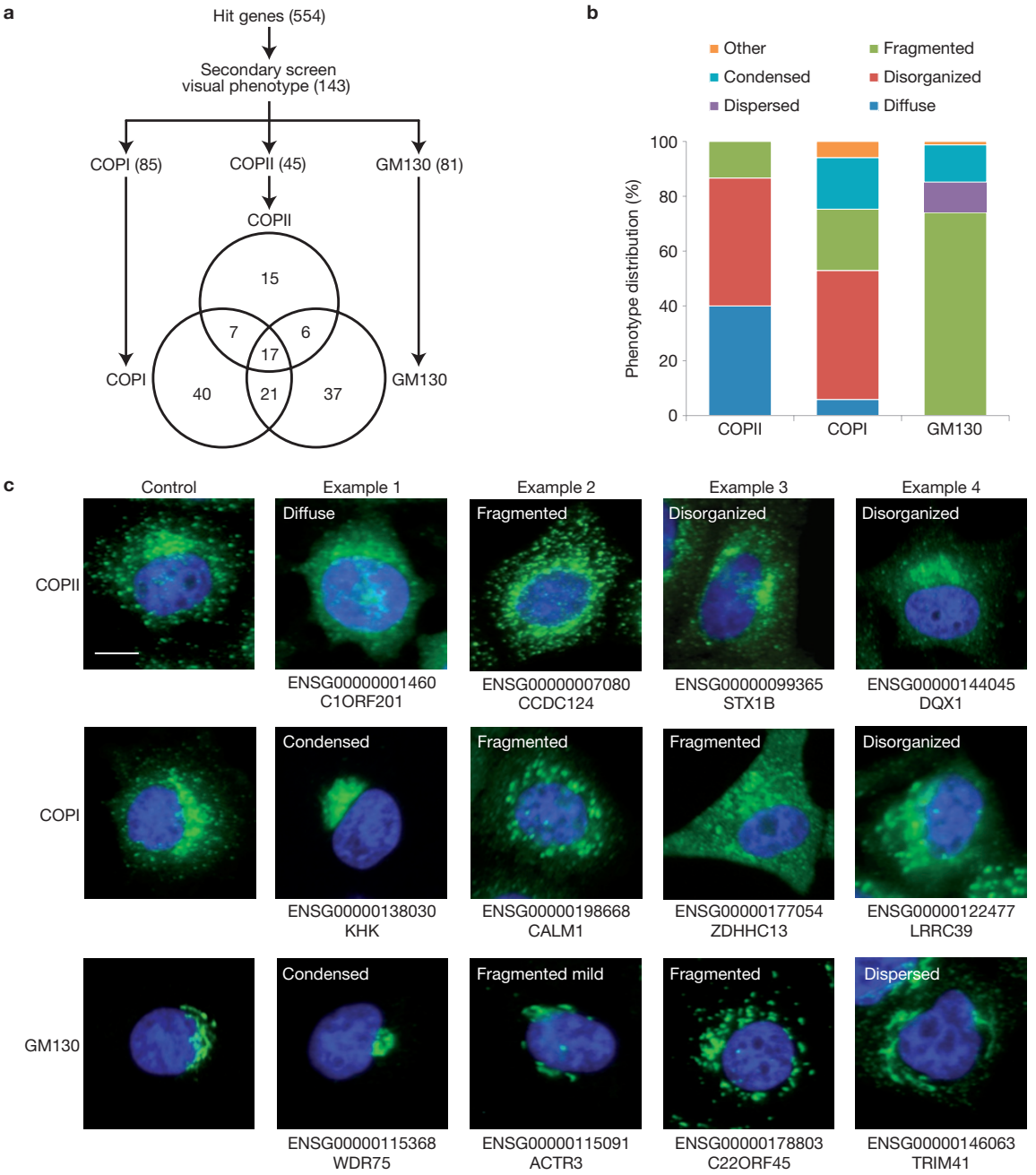

Figure 5 Secondary screening analysis of the hit genes identified in the secretion screens. (**a**) Overview of the numbers of genes having an effect on the distribution or appearance of either the COPII coat, COPI coat or the Golgi matrix protein GM130 after 50 h downregulation, as determined by visual analysis. (**b**) Distribution of the phenotypes observed for the 143 genes recorded as having effects in the secondary screens. (**c**) Example immunostainings of cells showing phenotypic effects on COPII, COPI or GM130. Scale bar, 10 μm. See also Supplementary Table S13.

seen in a complete proteome (Fig. 4d). One explanation for this is that mammalian systems contain a more extensive and specialized endomembrane system[36]; however, we consider it more likely that our secretion screen has enriched for proteins associated with and functioning in the secretory pathway. Consistent with this, we recorded a reduced representation of proteins associated with mitochondria and the nucleus (Fig. 4d).

Morphological changes to early secretory pathway membranes

To more specifically assign the genes identified in our primary and validation secretion screens to their organelle or functional module we performed secondary RNAi-based screens on our 554 hit genes, with a particular focus on identifying components of the early secretory pathway (ER and Golgi complex). We visually assessed the COPII and COPI coats, and the Golgi matrix protein GM130 (as an indicator of Golgi integrity) by immunostaining. This analysis revealed phenotypes for 143 of the hit genes (Fig. 5a and Supplementary Table S13), which we then classified as either diffuse, disorganized, fragmented, dispersed or condensed (Fig. 5b,c and Methods). A small number of phenotypes observed did not fit this classification system, and were denoted as other. The most abundant phenotype observed for the COPII coat was disorganized,

in which punctate ER exit sites could still be discriminated, but their distribution through the cytoplasm was perturbed (for example STX1B, Fig. 5c). Several of the genes on knockdown resulted in an increased cytoplasmic appearance of the COPII and COPI coat complexes (for example, C1ORF201 and ZDHHC13) or a compaction/condensing of the coats and membranes (for example, KHK and WDR75), but the most common phenotypic profile was that of fragmentation (for example, CALM1 and C22ORF45, Fig. 5c). This visual phenotypic profiling within the endomembrane system is particularly useful to increase our understanding of the potential function of the molecules. For example, the Golgi complex maintains its specific juxta-nuclear morphology as a result of the proteins that coat these membranes and through interactions with the underlying cytoskeleton. Perturbations in either of these classes of molecules often result in Golgi fragmentation, a phenotype that we commonly recorded. Similarly, coat proteins undergo repeated rounds of membrane association and dissociation as part of their normal cycling activity, and therefore the compaction phenotypes observed suggest a role in coat dissociation from membranes; conversely diffuse phenotypes suggest a role in coat recruitment to membranes. However, this type of analysis does not report the potential strength or importance of each newly identified protein to the marker of interest. Therefore, to make our secondary screening data quantitative, we applied texture-based image analysis algorithms to the cells showing phenotypes, followed by Mahalanobis distance calculations to assess the relative change in COPII, COPI and GM130 distributions when compared with control cells (see Methods). This approach allowed us to rank the strength of each phenotype, thereby providing us with a further tool with which to prioritize their characterization (Supplementary Table S13).

Network analysis of secretion regulators

We next sought to identify whether any of the proteins identified in our screens could be mapped to a functional network. Focusing on the lists of hit genes affecting secretion and early secretory pathway morphology, and for which we had subcellular localization information, we used the STRING database of interactions[37] to reveal a number of networks. The first of these networks contained several Rab family small GTP-binding proteins and two members of the Ras family (HRAS and NRAS), all centred on RABAC1 (also known as PRA1, PRAF1 and YIP3; Fig. 6a). RABAC1 is a transmembrane protein that was initially reported to play a counter role to Rab–GDI molecules, restricting the solubilization of membrane-bound Rab GTPases (ref. 38). Subsequent work showed that RABAC1 is capable of catalytically dissociating GDI-bound endosomal Rabs and delivering them to appropriate membranes[39], making it a strong candidate as a core piece of membrane traffic machinery. RABAC1 interacts with various GTPases and viral proteins, and has been suggested to link membrane traffic to signalling[40]. In our experiments, depletion of RABAC1 mildly inhibited secretion, and caused mild morphological changes to the COPII and COPI coats (Fig. 6a,c). Overexpression of wild-type RABAC1 has also been shown to reduce the rate of ER-to-Golgi traffic of tsO45G (ref. 41). Our observations of altered early secretory pathway coat complex morphologies in RABAC1 knockdown cells was a little surprising, as RABAC1 has largely been implicated to function at Golgi, post-Golgi and endosomal membranes. Nevertheless, the fact that it interacts with Rabs found throughout the secretory pathway, including some at the ER–Golgi interface (RAB1A), suggests that this molecule may provide a hub for secretory traffic organization.

A second network of interest was centred on another GTPase-interacting protein, namely the RAP1 GTP–GDP dissociation stimulator 1 protein (RAP1GDS1), alternatively known as SmgGDS (Fig. 6b). RAP1GDS1 is an atypical guanine nucleotide exchange factor involved in the activation of various GTPases from the Ras and Rho subfamilies, with recent work suggesting that it can control the prenylation and therefore membrane localization of Rap1A, RhoA and Rac1 GTPases[42]. Although these GTPases ultimately reside at or close to the plasma membrane, they undergo a post-prenylation processing event at the ER (ref. 43). Our screens revealed that RNAi of RAP1GDS1 resulted in decreased secretory activity, and a reorganization of COPII-coated ER exit sites into a more diffuse appearance (Fig. 6c). Although subcellular localization analysis of RAP1GDS1 indicated it to be a soluble molecule, our functional data suggest that this protein is a key regulator of secretory activity, probably acting in the early secretory pathway.

A third notable network that we were able to discern was focused around a GTPase regulator, SOS2 (son of sevenless homologue 2; Fig. 6d). The SOS2 protein possesses guanine nucleotide exchange activity towards Ras proteins and participates in signalling events emanating from receptor tyrosine kinases[44]. This network also contained molecules associated with epidermal growth factor (EGF) signalling, including the EGF receptor itself, in addition to Rho GTPase function. This network was particularly striking because some members, including the atypical Rho GTPase RHOU and two Rho GTPase-activating proteins (GAPs) ARHGAP12 and ARHGAP44 (also known as RICH2), in addition to SOS2, resulted in phenotypic effects on the early secretory pathway on knockdown. In each of these cases we observed a change in the distribution of COPII-coated ER exit sites when compared with control cells (Fig. 6e). Analysis of the actin cytoskeleton in these cells also revealed phenotypic effects, with knockdown of RHOU resulting in an increase in the number of stress fibres, an observation consistent with previous reports[45] (Fig. 6f). In contrast, depletion of the two GAPs resulted in changes in cell morphology, a marked loss of F-actin, and actin accumulation in short disorganized bundles (Fig. 6f). A similar phenotype has been reported for ARHGAP44 depletion in polarized Caco-2 cells[46]. Interestingly, NRAS was part of all three networks identified, linking them functionally together as a central hub.

Functional link between EGF stimulation and secretory pathway function

Altogether these analyses strongly suggested the presence of so far unappreciated critical network links between secretory pathway function and small GTP-binding protein regulation, actin cytoskeleton organization and EGF-mediated signalling from the cell surface. As the knockdown of members of these networks, including the EGF receptor itself, caused a secretion inhibition, we predicted that the stimulation of cells with EGF might increase the efficiency of the secretory pathway through activation of any or indeed all of these network partners. Cells were stimulated for two hours with EGF, or PDGF as a control, before carrying out tsO45G transport

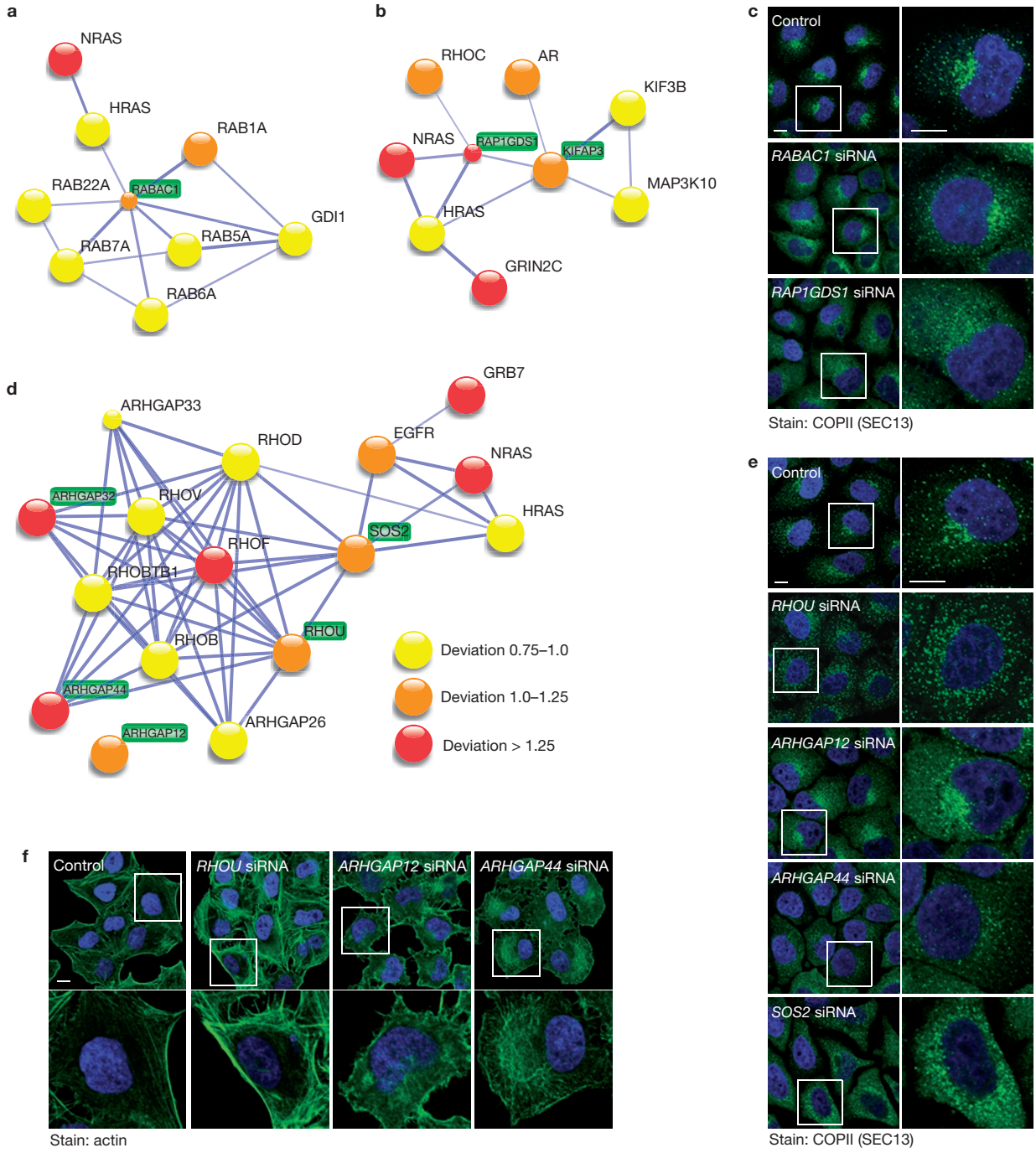

Figure 6 Characterization of selected networks of genes identified as being important for regulation of secretion. (**a**) Network of small GTP-binding proteins found to be important for secretion and centred round the Rab acceptor 1 protein (RABAC1) as determined by STRING analysis. (**b**) Network of proteins found to be important for secretion and centred round the RAP1 GTP–GDP dissociation stimulator 1 protein (RAP1GDS1) as determined by STRING analysis. (**c**) Immunostainings of COPII-coated ER exit sites (labelled for SEC13) in the presence of various siRNAs targeting genes in the networks of **a** and **b**. (**d**) Network of cytoskeleton regulatory proteins found to be important for secretion and centred around SOS2 as determined by STRING analysis. In **a**,**b** and **d** those genes also producing phenotypes in the secondary screens are highlighted in green. The strength of secretion inhibition is denoted by the colours of the nodes, and the size of each node indicates the relative availability of structural information for domains within each protein. The thickness of lines connecting nodes indicates the confidence in the protein associations. (**e**) Immunostainings of COPII-coated ER exit sites (labelled for SEC13) in the presence of various siRNAs targeting genes in the network of **d**. (**f**) Appearance of the actin cytoskeleton in the presence of various siRNAs targeting genes in the network of **d**. For all images both an overview of several cells and an individual cell (marked with a square) are shown. Scale bars, 10 μm.

experiments. Whereas the efficiency (amount on cell surface relative to total amount present in the cell) of transport of tsO45G was only marginally increased in EGF-stimulated cells when compared with PDGF- or non-treated cells (Fig. 7a), the total amount of cell surface tsO45G was significantly increased (Fig. 7b). This indicates that specifically in EGF-treated cells, the secretory machinery is

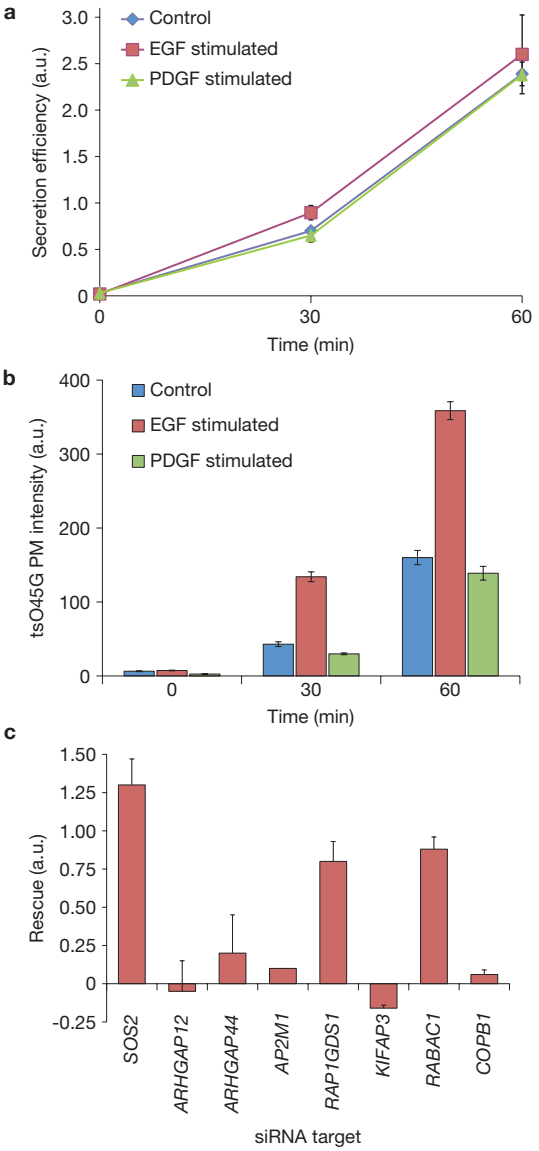

Figure 7 Functional link between EGF stimulation and secretory pathway function. (**a**) Effect on secretion efficiency (cell surface tsO45G/total tsO45G) in HeLa cells stimulated for 2 h with either 100 ng ml^{-1} EGF or PDGF ($n = 3$). (**b**) Effect of EGF or PDGF treatment on the total amount of tsO45G reaching the cell surface in HeLa cells ($n = 4$). (**c**) Rescue of secretion in HeLa cells downregulated for the genes indicated when exposed to EGF. Rescue was calculated by the following formula: Rescue (a.u.) = [Inhibition (−EGF) − Inhibition (+EGF)]/Inhibition (−EGF) ($n = 3$, with the exception of the AP2M1 knockdown where $n = 2$). Bars indicate mean and standard deviations between replicate experiments; a.u., arbitrary units.

activated and experiences an increased load. One explanation for the lack of effect of EGF stimulation on the efficiency with which tsO45G is transported to the plasma membrane could be that under our experimental conditions, the secretory pathway may already be saturated. To test this, cells were treated with siRNAs targeting members of the identified network to generate conditions of sub-optimum transport efficiency, before stimulation with EGF. Strikingly, we observed that for some siRNA treatments, EGF stimulation could markedly increase the transport efficiency when compared with control siRNA-treated cells, and in the case of cells depleted for SOS2, transport of tsO45G to the plasma membrane could be completely restored (Fig. 7c). No such rescue of transport could be seen for cells stimulated with PDGF (not shown). Partial rescue of transport by EGF could also be obtained in RAP1GDS1 and RABAC1 knockdown cells, whereas this rescue was not observed in cells depleted for genes encoding COPB1 and AP2M1, which play a structural role within the membrane traffic process.

DISCUSSION

This study is the most comprehensive assessment of genes associated with secretory pathway function in metazoans so far. Using a systematic RNAi strategy we provide a global analysis of gene function with respect to the constitutive secretion of a model transmembrane protein, revealing that more than 15% of the genome encodes proteins that can be linked to this fundamental cellular process. Our analyses indicate that in higher eukaryotes the regulation of the secretory pathway occurs at multiple levels. Alongside the well-established core machinery, it involves cross-talk with small GTP-binding protein regulation, actin cytoskeleton organization and EGF-mediated signalling from the cell surface. Surprisingly, the GTPases discovered in our screens were not just the well-established regulators of membrane traffic events, but included Rho and Ras family proteins and their regulatory networks. Together, this implies that mammalian cells have evolved a highly sophisticated signalling and feedback system that allows them to modulate their secretory activity in response to external signals and their local environment[47]. The challenge now is to understand how these events in the cell periphery directly modulate the secretion machinery at the level of the ER and Golgi complex. The data presented in this work provide the basic tools to undertake this task. □

METHODS

Methods and any associated references are available in the online version of the paper at www.nature.com/naturecellbiology

Note: Supplementary Information is available on the Nature Cell Biology website

ACKNOWLEDGEMENTS

We thank OSIS, Olympus Europe and the ALMF team at EMBL, Heidelberg for support. In addition, we acknowledge technical and bioinformatic help from J. Bulkescher, C. Conrad, U. Liebel, P. Rogers, C. Tischer and T. Walter. This project was financially supported by grants to J.E. within the MitoCheck consortium by the European Commission (FP6-503464) as well as by the Federal Ministry of Education and Research (BMBF) in the framework of the National Genome Research Network (NGFN) (NGFN-2 SMP-RNAi, FKZ01GR0403); and R.P. and S.W. (BMBF NGFN2 SMP-Cell and NGFN-Plus IG-CSG); and R.P. (Baden Württemberg Stiftung, Germany, Programme 'siRNA'). The R.P. laboratory is also supported by the EU-funded network of excellence 'Systems Microscopy'. A.M. was supported by a fellowship of the programme de Becas de Especialización en Organismos Internacionales of the Spanish Ministry of Education and Science (MEC). The J.C.S. laboratory is supported by a Principal Investigator (PI) award (09/IN.1/B2604) from Science Foundation Ireland (SFI).

AUTHOR CONTRIBUTIONS

J.C.S. and R.P. designed the study and prepared the manuscript. J.C.S., B.J., V.L., F.V., H.E., M.G.B., J.B. and S.B. performed experiments; J.C.S., C.C., V.R.S., J-K.H., B.N., A.M. and R.P. analysed data; and V.B., S.W. and J.E. provided critical advice. All authors commented on the manuscript at the preparation stages.

COMPETING FINANCIAL INTERESTS

The authors declare no competing financial interests.

Published online at www.nature.com/naturecellbiology
Reprints and permissions information is available online at www.nature.com/reprints

1. Behnia, R. & Munro, S. Organelle identity and the signposts for membrane traffic. *Nature* **438,** 597–604 (2005).
2. Bonifacino, J. S. & Glick, B. S. The mechanisms of vesicle budding and fusion. *Cell* **116,** 153–166 (2004).
3. Lee, M. C. & Miller, E. A. Molecular mechanisms of COPII vesicle formation. *Semin. Cell Dev. Biol.* **18,** 424–434 (2007).
4. Beck, R., Rawet, M., Wieland, F. T. & Cassel, D. The COPI system: molecular mechanisms and function. *FEBS Lett.* **583,** 2701–2709 (2009).
5. Simpson, J. C. Screening the secretion machinery: high throughput imaging approaches to elucidate the secretory pathway. *Semin. Cell Dev. Biol.* **20,** 903–909 (2009).
6. Gilchrist, A. *et al.* Quantitative proteomics analysis of the secretory pathway. *Cell* **127,** 1265–1281 (2006).
7. Bard, F. *et al.* Functional genomics reveals genes involved in protein secretion and Golgi organization. *Nature* **439,** 604–607 (2006).
8. Wendler, F. *et al.* A genome-wide RNA interference screen identifies two novel components of the metazoan secretory pathway. *EMBO J.* **29,** 304–314 (2010).
9. Farhan, H. *et al.* MAPK signaling to the early secretory pathway revealed by kinase/phosphatase functional screening. *J. Cell Biol.* **189,** 997–1011 (2010).
10. Gordon, D. E., Bond, L. M., Sahlender, D. A. & Peden, A. A. A targeted siRNA screen to identify SNAREs required for constitutive secretion in mammalian cells. *Traffic* **11,** 1191–1204 (2010).
11. Simpson, J. C. *et al.* An RNAi screening platform to identify secretion machinery in mammalian cells. *J. Biotechnol.* **129,** 352–365 (2007).
12. Neumann, B. *et al.* Phenotypic profiling of the human genome by time-lapse microscopy reveals cell division genes. *Nature* **464,** 721–727 (2010).
13. Zilberstein, A., Snider, M. D., Porter, M. & Lodish, H. F. Mutants of vesicular stomatitis virus blocked at different stages in maturation of the viral glycoprotein. *Cell* **21,** 417–427 (1980).
14. Sato, K. & Nakano, A. Mechanisms of COPII vesicle formation and protein sorting. *FEBS Lett.* **581,** 2076–2082 (2007).
15. Wendeler, M. W., Paccaud, J. P. & Hauri, H. P. Role of Sec24 isoforms in selective export of membrane proteins from the endoplasmic reticulum. *EMBO Rep.* **8,** 258–264 (2007).
16. Scales, S. J., Pepperkok, R. & Kreis, T. E. Visualization of ER-to-Golgi transport in living cells reveals a sequential mode of action for COPII and COPI. *Cell* **90,** 1137–1148 (1997).
17. Stephens, D. J., Lin-Marq, N., Pagano, A., Pepperkok, R. & Paccaud, J. P. COPI-coated ER-to-Golgi transport complexes segregate from COPII in close proximity to ER exit sites. *J. Cell Sci.* **113,** 2177–2185 (2000).
18. Gurkan, C. *et al.* Large-scale profiling of Rab GTPase trafficking networks: the membrome. *Mol. Biol. Cell* **16,** 3847–3864 (2005).
19. Dejgaard, S.Y. *et al.* Rab18 and Rab43 have key roles in ER–Golgi trafficking. *J. Cell Sci.* **121,** 2768–2781 (2008).
20. Nuoffer, C., Davidson, H. W., Matteson, J., Meinkoth, J. & Balch, W. E. A GDP-bound of rab1 inhibits protein export from the endoplasmic reticulum and transport between Golgi compartments. *J. Cell Biol.* **125,** 225–237 (1994).
21. Yang, C., Slepnev, V. I. & Goud, B. Rab proteins form *in vivo* complexes with two isoforms of the GDP-dissociation inhibitor protein (GDI). *J. Biol. Chem.* **269,** 31891–31899 (1994).
22. Plutner, H. *et al.* Rab1b regulates vesicular transport between the endoplasmic reticulum and successive Golgi compartments. *J. Cell Biol.* **115,** 31–43 (1991).
23. Iinuma, T. *et al.* Role of syntaxin 18 in the organization of endoplasmic reticulum subdomains. *J. Cell Sci.* **122,** 1680–1690 (2009).
24. Belgareh-Touzé, N. *et al.* Yeast functional analysis: identification of two essential genes involved in ER to Golgi trafficking. *Traffic* **4,** 607–617 (2003).
25. Uemura, T. *et al.* p31 deficiency influences endoplasmic reticulum tubular morphology and cell survival. *Mol. Cell. Biol.* **29,** 1869–1881 (2009).
26. Kim, J. *et al.* Functional genomic screen for modulators of ciliogenesis and cilium length. *Nature* **464,** 1048–1051 (2010).
27. Guo, Y. *et al.* Functional genomic screen reveals genes involved in lipid-droplet formation and utilization. *Nature* **453,** 657–661 (2008).
28. Jacquier, N. *et al.* Lipid droplets are functionally connected to the endoplasmic reticulum in Saccharomyces cerevisiae. *J. Cell Sci.* **124,** 2424–2437 (2011).
29. Pepperkok, R., Simpson, J. C. & Wiemann, S. Being in the right location at the right time. *Genome Biol.* **2,** 1024.1–1024.4 (2001).
30. Schnell, U., Dijk, F., Sjollema, K. A. & Giepmans, B. N. G. Immunolabeling artifacts and the need for live-cell imaging. *Nat. Methods* **9,** 152–158 (2012).
31. Simpson, J. C., Wellenreuther, R., Poustka, A., Pepperkok, R. & Wiemann, S. Systematic subcellular localisation of novel proteins identified by large-scale cDNA sequencing. *EMBO Rep.* **1,** 287–292 (2000).
32. Meng, X. *et al.* CLIC2-RyR1 interaction and structural characterization by cryo-electron microscopy. *J. Mol. Biol.* **387,** 320–334 (2009).
33. Singh, H., Cousin, M. A. & Ashley, R. H. Functional reconstitution of mammalian 'chloride intracellular channels' CLIC1, CLIC4 and CLIC5 reveals differential regulation by cytoskeletal actin. *FEBS J.* **274,** 6306–6316 (2007).
34. Huh, W. K. *et al.* Global analysis of protein localization in budding yeast. *Nature* **425,** 686–691 (2003).
35. Matsuyama, A. *et al.* ORFeome cloning and global analysis of protein localization in the fission yeast *Schizosaccharomyces pombe*. *Nat. Biotech.* **24,** 841–847 (2006).
36. Simpson, J. C. & Pepperkok, R. Localizing the proteome. *Genome Biol.* **4,** 240 (2003).
37. Szklarczyk, D. *et al.* The STRING database in 2011: functional interaction networks of proteins, globally integrated and scored. *Nucleic Acids Res.* **39,** D561–D568 (2011).
38. Hutt, D. M., Da-Silva, L. F., Chang, L. H., Prosser, D. C. & Ngsee, J. K. PRA1 inhibits the extraction of membrane-bound rab GTPase by GDI1. *J. Biol. Chem.* **275,** 18511–18519 (2000).
39. Sivars, U., Aivazian, D. & Pfeffer, S. R. Yip3 catalyses the dissociation of endosomal Rab–GDI complexes. *Nature* **425,** 856–859 (2003).
40. Liu, H. P., Wu, C. C. & Chang, Y. S. PRA1 promotes the intracellular trafficking and NF-kappaB signaling of EBV latent membrane protein 1. *EMBO J.* **25,** 4120–4130 (2006).
41. Gougeon, P. Y., Prosser, D. C., Da-Silva, L. F. & Ngsee, J. K. Disruption of Golgi morphology and trafficking in cells expressing mutant prenylated rab acceptor-1. *J. Biol. Chem.* **277,** 36408–36414 (2002).
42. Berg, T. J. *et al.* Splice variants of SmgGDS control small GTPase prenylation and membrane localization. *J. Biol. Chem.* **285,** 35255–35266 (2010).
43. Wright, L. P. & Philips, M. R. Thematic review series: lipid posttranslational modifications. CAAX modification and membrane targeting of Ras. *J. Lipid Res.* **47,** 883–891 (2006).
44. Rojas, J. M., Oliva, J. L. & Santos, E. Mammalian son of sevenless Guanine nucleotide exchange factors: old concepts and new perspectives. *Genes Cancer* **2,** 298–305 (2011).
45. Chuang, Y. Y., Valster, A., Coniglio, S. J., Backer, J. M. & Symons, M. The atypical Rho family GTPase Wrch-1 regulates focal adhesion formation and cell migration. *J. Cell Sci.* **120,** 1927–1934 (2007).
46. Rollason, R., Korolchuk, V., Hamilton, C., Jepson, M. & Banting, G. A CD317/tetherin-RICH2 complex plays a critical role in the organization of the subapical actin cytoskeleton in polarized epithelial cells. *J. Cell Biol.* **184,** 721–736 (2009).
47. Farhan, H. & Rabouille, C. Signalling to and from the secretory pathway. *J. Cell Sci.* **124,** 171–180 (2011).

METHODS

Primary and validation secretion screens. All siRNAs used in the primary screen were from Ambion, and in the validation and secondary screens from Ambion and Qiagen. These libraries are further described elsewhere[12]. The genome-wide library was arrayed into a total of 149 chambered coverglass slides at a density of 384 siRNA spots per chamber. All primary screen chambers contained between 1 and 4 positive control siRNAs against the β-COP (COPB1) subunit of the vesicular coat protein complex COPI, in addition to 7–8 non-silencing negative control siRNAs, all previously described[11]. The validation screen arrays contained a total of 44 controls, as follows. 16 spots of negative control siRNA, 4 spots of siRNA against INCENP to mark the extreme corners of the arrays, 8 spots of siRNA against COPB1, 8 spots of siRNA against GOSR1 (Ambion ID 111531) and 8 spots of siRNA against RAB1A (Ambion ID 120368; refs 11,12,48).

HeLa Kyoto cells were used for all experiments. The design, implementation and quantification of the tsO45G assay in array format have been described in detail previously[11]. All images were acquired on a fully automated Olympus Scan^R screening microscope. At the end of each experiment the cell plating density of every chamber was visually assessed, and those arrays showing obvious edge or cell density effects were excluded from quantification. Secretory transport was calculated from individual cells by determining the ratio of cell surface tsO45G to total tsO45G. Mean values per spot were converted into deviation scores, with values >0.75–1.00 indicating mild reduction of cell surface tsO45G delivery, values >1.0 indicating strong reduction of cell surface tsO45G delivery, and values < -1 indicating enhanced cell surface tsO45G delivery. All other values were considered as no effect. Secretion deviation values in the validation screen were determined from the formula $(T_{control} - T_{experiment})/2 \times s.e.m._{control}$, where T is the ratio of cell surface tsO45G to total tsO45G. Quality control thresholds were applied to the data from the primary and validation screens as follows. A minimum of 15 cells per spot needed to be recognized by the analysis software if the spot was to be considered valid and used for quantification. A minimum of 50 cells from all replicate chambers was the minimum number for consideration of the siRNA giving reliable information. The siRNAs were considered as inhibitory to secretion only when >= 50% of the replicates (that is 2/2, 2/3, 3/3, 2/4, 3/4, 4/4, 3/5, 4/5, 5/5 and so on) had matching deviation values (0.75–1.00 or >1.0). Data from siRNAs mapping to multiple genes, or showing any mismatches, were removed from the analysis as part of the quality control process. The siRNAs were mapped to Ensembl version *e*!61. The data from the primary and validation screens are all available at www.mitocheck.org.

Secondary screens for organelle morphology. HeLa Kyoto cells were incubated on siRNA arrays for a total of 50 h before fixing with either methanol or 3% paraformaldehyde, followed by immunostaining using standard methods. The arrays used for these experiments contained the same set of siRNAs used in the validation screen. The product identifiers of the siRNAs giving the strongest positive phenotypes in these screens are listed in Supplementary Table S13. For a small number of the genes targeted, predesigned siRNAs were not available. In these cases the target sequence against which the custom siRNA was designed is also given in this Table. Primary antibodies were against the COPII subunit SEC13 (rabbit polyclonal, this study, used at 1:50 dilution), the COPI subunit COPB2 (refs. 49; used at 1:400 dilution) and the matrix protein GM130 (clone 35/GM130, cat. no. 610822, used at 1:500 dilution; BD Biosciences). Fluorescently conjugated secondary antibodies (A-11029, A-11034, A-11031 and A-11036 were used at 1:800 dilution; A-21236 and A-21245 were used at 1:400 dilution) were from Life Technologies/Molecular Probes. Images were acquired on a fully automated Olympus Scan^R screening microscope with a ×20/0.75 NA UPlanSApo objective, and were visually inspected for phenotypic changes to organelle morphologies. The COPII and COPI coats were annotated as either wild type (no effect); disorganized (indicating the presence of distinct punctate structures, but lacking their normal juxta-nuclear enrichment); diffuse (indicating reduced number of punctate structures, but an increase in soluble signal); or fragmented (indicating the presence of distinct punctate structures, but of uneven sizes). The COPI coat was also annotated as either condensed (indicating lack of punctate structures but enriched in a single concentrated region of the cell); enlarged (indicating an increased number or intensity of structures); or tubulated (indicating an enlargement in the area of juxta-nuclear signal alone). GM130 was annotated as either wild type (no effect); fragmented (indicating loss of juxta-nuclear signal, but presence of signal in fragments distributed throughout cytoplasm); fragmented mild (indicating partial loss of juxta-nuclear signal, and presence of further fragments in cytoplasm); dispersed (indicating presence of juxta-nuclear signal, but with a loss in its usual compactness); condensed (indicating an enrichment in a single concentrated region of the cell); or enlarged (indicating an increased number or intensity of structures).

The relative strengths of the phenotypes observed were also quantified using customized ImageJ software, specifically measuring Haralick texture features, granularity, level set features and intensity-based features for all cells manually annotated as exhibiting the phenotypes described above. Cells with aberrant-shaped nuclei (determined from 7 shape features including area, convex hull area and circularity factors) were disregarded using an expectation maximization clustering method. Next a covariance matrix of 24 non-correlated features was generated, and this was then used to calculate the Mahalanobis distance[50], allowing us to measure the distance of each experimental cell from control cells. This approach has the advantage that it is scale-invariant, so any feature with high mean value will not carry additional weight compared with a feature with low mean value. The mean Mahalanobis distance (MD) for each siRNA was then determined and the secondary screen deviation compared with control cells was then calculated according to the formula $(\text{mean MD}_{control} - \text{mean MD}_{experiment})/2 \times \text{s.d.}_{control}$.

RT–qPCR. Following siRNA treatment, cells grown in 12-well plates were collected and total RNA prepared using an InviTrap Spin Cell RNA Mini Kit (Stratec Molecular). For reverse transcription reactions, 1 μg of total RNA was reverse transcribed using a High Capacity cDNA Reverse Transcription Kit (Applied Biosystems), and quantitative PCR (qPCR) analysis was carried out using SYBR green detection in an Applied Biosystems 7500 system, all according to the manufacturer's protocols. The qPCR cycling conditions were set up as follows: holding stage 50 °C/20 s, 95 °C/10 min (1 cycle); cycling stage 95 °C/15 s, 60 °C/1 min (40 cycles); melting curve stage 95 °C/15 s, 60 °C/1 min, 95 °C/30 min, 60 °C/15 s (1 cycle).

Transcriptome sequencing. An RNA sequencing library was prepared from HeLa Kyoto cell total RNA using an mRNA-Seq 8-Sample Prep Kit (Illumina). The resulting library was sequenced for 36 cycles and 76 cycles on an Illumina GAII and GAIIx machine respectively according to the manufacturer's instructions. Sequence data were processed using GA-pipeline 1.4.0 software (Illumina) resulting in 4,695,921 aligned reads for the 36 base run and 10,294,425 aligned reads for the 76 base run. Alignments were performed using ELAND software against the hg19 genome build and RNASeq analysis was performed using Genomatix RegionMiner software (www.genomatix.de). The resulting data showed a 26-fold enrichment for exonic regions in the 36 and 23-fold in the 76 base runs. The resulting expression profiles of read counts per transcript were mapped to transcripts under investigation using Perl scripts.

Cloning and subcellular localization of proteins. The selection of which ORFs to clone was primarily based on two criteria, namely the novelty of the protein with respect to its role in secretory membrane traffic (according to literature searches), and the availability of a source cDNA. ORFs of interest were cloned into ECFP and EYFP expression vectors using Gateway recombination cloning (Life Technologies), and transfected into HeLa Kyoto cells as described previously[31]. Initial analysis of localization was made in living cells by manual inspection of the respective transfected cell cultures and representative images from a minimum of 10 transfected cells were acquired and used to positively annotate localization. Where N-terminal and C-terminal localization patterns did not correspond, preference in annotation was always given to membrane structures versus soluble patterns[31]. Bioinformatic resources were also used to assist annotation as required. Where necessary cells were then fixed and immunostained with appropriate antibodies (mouse monoclonal anti-α-tubulin, clone DM1A, catalogue no. MS-581-P, used at 1:500 dilution; Neomarkers) or stains (phalloidin–AlexaFluor647, catalogue no. A-22287, used at 1:40 dilution; Life Technologies). Confocal images were acquired on an Olympus FV1000 microscope with a ×60/1.35 NA UPlanSApo oil immersion objective. Sequential scanning of channels was always used during acquisition.

EGF experiments. HeLa cells infected with recombinant adenoviruses encoding tsO45G (ref. 12) were treated for 2 h at 39.5 °C with 100 ng ml^{-1} of either EGF or PDGF (control cells remained untreated) before being shifted to 32 °C for various times before they were fixed and immunostained for tsO45G at the plasma membrane. The secretion efficiency (cell surface tsO45G/total tsO45G) as a function of time at 32 °C was calculated.

EGF rescue experiments. HeLa Kyoto cells were grown on 8-well Lab-Tek chambers (Nunc, Thermo Scientific) for 16 h in complete medium. They were then transfected with either negative control siRNAs, or siRNAs targeting SOS2, ARHGAP12, ARHGAP44, AP2M1, RAP1GDS1, KIFAP3, RABAC1 or COPB1 (Ambion) using Oligofectamine transfection reagent (Invitrogen) according to the manufacturer's instructions. Final siRNA concentrations were 20 nM for all siRNAs except RABAC1, which required 90 nM. Forty-eight hours later the cells were infected with recombinant adenoviruses encoding tsO45G–YFP. After 60 min the adenoviruses were washed away, the cells were held at 39.5 °C for 4 h to accumulate the tsO45G–YFP in the ER, then either not stimulated (untreated control cells) or stimulated with EGF (100 ng ml^{-1}; Sigma-Aldrich, Munich, Germany) or PDGF (100 ng ml^{-1}; Sigma-Aldrich) and held at 39.5 °C for a further 2 h. Cells were then shifted to 32 °C to release the tsO45G–YFP from the ER in the presence of cycloheximide (100 μg ml^{-1}) and 25 mM HEPES. After 30 min, the cells were fixed with 3.5% paraformaldehyde (without permeabilization)

DOI: 10.1038/ncb2510

and processed as described for the primary screen[11]. Images were acquired on an automated Olympus Scan^R microscope with a UPlanAPO 20×/0.7 NA air objective. Sufficient images to contain approximately 3,000 cells in total were typically acquired for each condition. The tsO45G secretion efficiency was calculated from individual cells by determining the transport rate as the ratio of the signal of tsO45G at the plasma membrane (Cy5 signal intensity) to the total tsO45G (YFP signal intensity) as described previously[12]. Transport inhibition was then calculated by the formula: mean transport rate [(control siRNA) − mean transport rate (siRNA)]/mean transport rate (control siRNA). Rescue was then calculated using the formula: Rescue (au) = [Inhibition(−EGF) − Inhibition(+EGF)]/Inhibition(−EGF). A minimum of two independent rescue experiments were performed for each siRNA.

Network analysis. Selected candidate genes identified from the screen as causing inhibition of secretion and changes in early secretory pathway morphology were analysed using the STRING interaction database (http://string-db.org; ref. 37). Initially we inputted lists of genes identified from the secondary screens, and then used STRING to determine the first level of interactors from these hubs. The secretion inhibition scores from these first level interactors were recorded, and if they scored as inhibitors, a further level of interactors was determined. Search parameters were set at medium confidence (0.400) and greater, and text mining was excluded from the prediction method. Networks were visualized in confidence view mode, with the line thicknesses indicating the level of confidence, and the size of each node indicating the relative availability of structural information for domains within each protein.

48. Erfle, H. *et al*. Reverse transfection on cell arrays for high content screening microscopy. *Nat. Protoc.* **2,** 392–399 (2007).
49. Lowe, M. & Kreis, T. E. *In vitro* assembly and disassembly of coatomer. *J. Biol. Chem.* **270,** 31364–31371 (1995).
50. Mahalanobis, P. On the generalized distance in statistics. *Proc. Natl Inst. Sci. India* **2,** 49–55 (1936).

DOI: 10.1038/ncb2510

nature cell biology

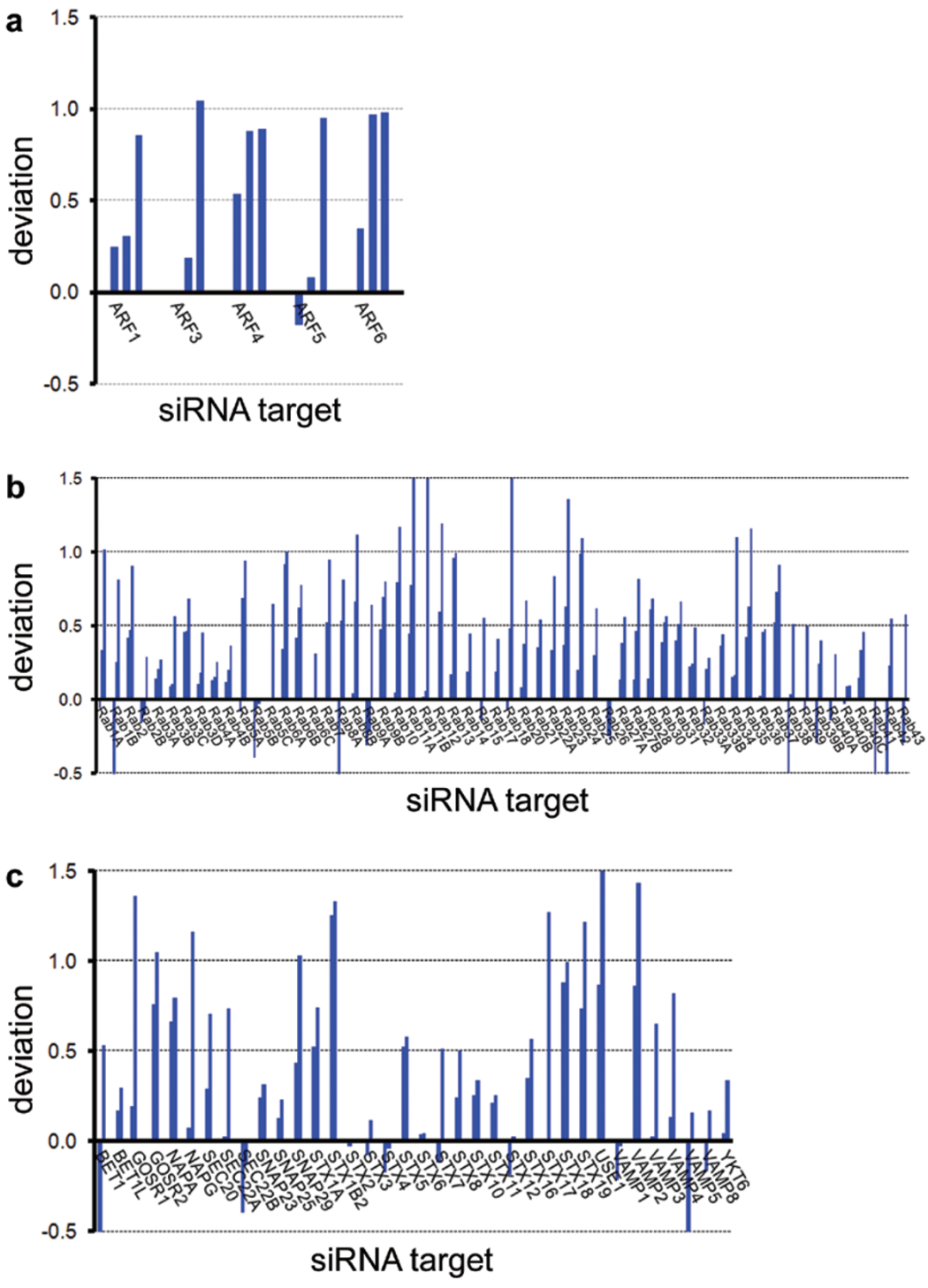

Figure S1 Effect on secretion of downregulation of known membrane traffic machinery molecules. (**a**) Effect of down-regulation of ARF GTPases on secretion. Secretion deviation values from the primary siRNA screen are shown for three independent siRNAs targeting each of the ARF GTPase family members. (**b**) Effect of down-regulation of Rab GTPases on secretion. Secretion deviation values from the primary siRNA screen are shown for two, or three when available, independent siRNAs targeting each of the Rab GTPase family members. (**c**) Effect of down-regulation of SNARE fusion molecules on secretion. Secretion deviation values from the primary siRNA screen are shown for two independent siRNAs targeting each of the SNARE fusion molecules. All siRNAs shown were from Ambion, and details of the siRNA sequences causing strongest inhibition are given in Supplementary Table S6. In all panels the individual bars represent data from individual siRNAs.

Supplementary Tables

Table S1 Secretion inhibitors from the primary screen after quality control for replicates, cell numbers, and siRNA mapping. Genes are listed by HGNC gene name (GENE SYMBOL). Also given are the ENSEMBL gene identifier (ENSEMBL ID) and siRNA manufacturer's identifier (siRNA ID). All siRNAs listed in this table were from Ambion. 'DEVIATION' indicates the strength of secretion inhibition, 'CELL NUMBER' indicates the number of cells quantified, 'VALID PLATES' indicates the number of replicate arrays used to determine the deviation, and '% INHIBITOR' indicates the proportion of replicates with deviation values considered inhibitory. 'TRANSCRIPT HIT' refers to the number transcripts targeted by the particular siRNA, and 'TRANSCRIPT IDS' indicates the transcript identifiers.

Table S2 Secretion accelerators from the primary screen. Genes are listed by HGNC gene name (GENE SYMBOL). Also given is the siRNA manufacturer's identifier (siRNA ID). All siRNAs listed in this table were from Ambion. 'DEVIATION' indicates the strength of secretion acceleration, 'CELL NUMBER' indicates the number of cells quantified, 'VALID PLATES' indicates the number of replicate arrays used to determine the deviation, and '% ACCELERATOR' indicates the proportion of replicates with deviation values considered acceleratory (deviation < -1.0).

Table S3 siRNAs for which no results were recorded due to insufficient cells remaining at the end of the experiment. Genes are listed by HGNC gene name (GENE SYMBOL). Also given are the ENSEMBL gene identifier (ENSEMBL ID) and siRNA manufacturer's identifier (siRNA ID). All siRNAs listed in this table were from Ambion.

Table S4 Transcriptome sequencing-verified genes on knock-down inhibiting tsO45G secretion as determined by at least two independent siRNAs (hit genes). Genes are listed by HGNC gene name (GENE SYMBOL). Also given are the ENSEMBL gene identifier (ENSEMBL ID) and the gene description (DESCRIPTION). The normalised expression values from the two transcriptome sequencing runs (NORM. EXPR. 1 and 2) and the final expression classification annotated (EXPRESSED) are also indicated. ND indicates 'not determined'. The number of independent siRNAs causing a secretion inhibition phenotype is shown (siRNA NUMBER), along with details of each of these siRNAs and their strength of inhibition (siRNA ID, siRNA MANUFACTURER and siRNA DEVIATION columns). These columns are colour-coded for easy examination. Details of the screen phase are also given for these results - 'primary' indicates that this result was from the primary secretion screen; all other results were from the validation screen. Custom designed siRNAs are denoted 'custom' and the target sequence of the siRNA is given.

Table S5 Genes on knock-down inhibiting tsO45G secretion, but for which no transcripts could be detected from whole transcriptome sequencing. Genes are listed by HGNC gene name (GENE SYMBOL). Also given are the ENSEMBL gene identifier (ENSEMBL ID), the gene description (DESCRIPTION), and the number of independent siRNAs causing a secretion inhibition phenotype (siRNA NUMBER).

Table S6 Secretion screen results from known membrane traffic machinery molecules. Genes are listed by functional class (CLASS; coat, small GTPase, SNARE). Also given are the HGNC gene name (GENE SYMBOL), the ENSEMBL gene identifier (ENSEMBL ID), the siRNA manufacturer's identifier (siRNA ID) of the strongest inhibitory siRNA, and the strength of secretion inhibition (DEVIATION). All siRNAs listed in this table were from Ambion. In addition, the pair of oligonucleotides used for RT-qPCR analysis is also given (qPCR OLIGO LEFT OLIGO and qPCR RIGHT OLIGO). ND indicates 'not determined'.

Table S7 Genes on knock-down inhibiting tsO45G secretion also identified as inhibiting secretion in fly (*Drosophila melanogaster* S2 cells), as determined by Bard et al. (2006)[7] and Wendler et al. (2010)[8]. Given are the *Drosophila* gene names (Dm GENE NAME), FlyBase identifier (FLYBASE GENE), the HGNC orthologue gene name (Hs GENE SYMBOL), the ENSEMBL gene identifier (Hs ORTHOLOGUE ID), and the siRNA manufacturer's identifier (siRNA ID) of the strongest inhibitory siRNA. 'DEVIATION' indicates the strength of secretion inhibition, 'CELL NUMBER' indicates the number of cells quantified, 'VALID PLATES' indicates the number of replicate arrays used to determine the deviation, and '% INHIBITOR' indicates the proportion of replicates with deviation values considered inhibitory. All siRNAs listed in this table were from Ambion.

Table S8 Genes on knock-down inhibiting tsO45G secretion also identified as causing cell death, cell division or cell motility defects, as determined by Neumann et al. (2010)[12]. Genes are listed by HGNC gene name (GENE SYMBOL). Also given are the ENSEMBL gene identifier (ENSEMBL ID) and the cell division phenotype as reported by Neumann et al. (2010)[12]. All siRNAs listed in this table were from Ambion.

Table S9 Kinase and phosphatase genes on knock-down inhibiting tsO45G secretion also identified as influencing ER-Golgi recycling, as determined by Farhan et al. (2010)[9]. Genes are listed by functional class (FARHAN ET AL. CLASS; ER, Golgi, Mixed). Also given are the HGNC gene name (GENE SYMBOL), the GenBank accession number (GENBANK), the gene description (DESCRIPTION), the ENSEMBL gene identifier (ENSEMBL ID), the siRNA manufacturer's identifier (siRNA ID) of the strongest inhibitory siRNA, and the strength of secretion inhibition (DEVIATION). All siRNAs listed in this table were from Ambion.

Table S10 Genes on knock-down inhibiting tsO45G secretion also identified as influencing ciliogenesis, as determined by Kim et al. (2010)[26]. Genes are listed by functional class (KIM ET AL. CLASS; Positive, Negative). Also given are the HGNC gene name (GENE SYMBOL), the gene description (DESCRIPTION), the ENSEMBL gene identifier (ENSEMBL ID), the siRNA manufacturer's identifier (siRNA ID) of the strongest inhibitory siRNA, and the strength of secretion inhibition (DEVIATION). All siRNAs listed in this table were from Ambion.

Table S11 Genes on knock-down inhibiting tsO45G secretion also identified as influencing lipid droplet formation in fly (*Drosophila melanogaster* S2 cells), as determined by Guo et al. (2008)[27]. Given are the *Drosophila* genes (Dm GENE), the *Drosophila* gene names (Dm GENE NAME), the gene description (DESCRIPTION), the functional class (GUO ET AL. CLASS), the HGNC orthologue gene name (Hs GENE SYMBOL), the ENSEMBL gene identifier (Hs ORTHOLOGUE ID), the siRNA manufacturer's identifier (siRNA ID) of the strongest inhibitory siRNA, and the strength of secretion inhibition (DEVIATION). All siRNAs listed in this table were from Ambion.

Table S12 GFP-tagging and localisation data for genes inhibiting tsO45G secretion on knock-down. A total of 179 genes inhibiting secretion were selected and the open reading frames (ORFs) tagged with DNA encoding GFP variants. Fusion constructs were transfected into cells and the localisations of the expressed fluorescent proteins recorded. Genes are listed by HGNC gene name (GENE SYMBOL). Also given are the ENSEMBL gene identifier (ENSEMBL ID), the gene description (DESCRIPTION), the final subcellular localisation annotated (FINAL LOCALISATION), and the individual localisation results from both N- and C-terminal fusions. 'nd' indicates not determined. Also given are the results for each gene from the validation secretion screen (VALIDATION SCREEN HIT) and the whole transcriptome sequencing experiments (TRANSCRIPTOME).

Table S13 Secondary screening analysis of genes inhibiting tsO45G secretion on knock-down. Genes inhibiting tsO45G secretion were tested in secondary screening assays for effects on morphology of the COPII coat complex, the COPI coat complex, and the Golgi matrix protein GM130. Genes influencing early secretory pathway morphology are listed by HGNC gene name (GENE SYMBOL). Also given are the ENSEMBL gene identifier (ENSEMBL ID), the gene description (DESCRIPTION), the siRNA manufacturer (siRNA MANUFACTURER), the siRNA ID (siRNA ID) ('custom' denotes custom designed siRNAs, and the target sequence is given) and the recorded morphologies of the COPII, COPI and GM130 markers. The strengths of secondary screening phenotypes as measured by texture feature analysis (see Methods for details) are also given as deviation values from control cells (DEVIATION COPII/COPI/GM130), and are colour-coded for easy examination. The recorded GFP-localisation results (from Supplementary Table S12) are also given.